



HAL
open science

The West African Monsoon Dynamics. Part III: The Quasi-Biweekly Zonal Dipole

Flore Mounier, Serge Janicot, George N. Kiladis

► **To cite this version:**

Flore Mounier, Serge Janicot, George N. Kiladis. The West African Monsoon Dynamics. Part III: The Quasi-Biweekly Zonal Dipole. *Journal of Climate*, 2008, 21, pp.1911. 10.1175/2007JCLI1706.1 . hal-00770576

HAL Id: hal-00770576

<https://hal.science/hal-00770576>

Submitted on 10 Jun 2021

HAL is a multi-disciplinary open access archive for the deposit and dissemination of scientific research documents, whether they are published or not. The documents may come from teaching and research institutions in France or abroad, or from public or private research centers.

L'archive ouverte pluridisciplinaire **HAL**, est destinée au dépôt et à la diffusion de documents scientifiques de niveau recherche, publiés ou non, émanant des établissements d'enseignement et de recherche français ou étrangers, des laboratoires publics ou privés.

The West African Monsoon Dynamics. Part III: The Quasi-Biweekly Zonal Dipole

FLORE MOUNIER

LMD/IPSL, CNRS, Ecole Polytechnique, Palaiseau, France

SERGE JANICOT

LOCEAN/IPSL, IRD, Université Pierre et Marie Curie, Paris, France

GEORGE N. KILADIS

Physical Sciences Division, NOAA/Earth System Research Laboratory, Boulder, Colorado

(Manuscript received 25 September 2006, in final form 11 July 2007)

ABSTRACT

This paper presents an investigation of the mechanisms giving rise to the main intraseasonal mode of convection in the African monsoon during northern summer, here identified as the quasi-biweekly zonal dipole (QBZD). The QBZD is primarily characterized by a quasi-stationary zonal dipole of convection whose dimension is larger than the West African monsoon domain, with its two poles centered along the Guinean coast and between 30° and 60°W in the equatorial Atlantic. The QBZD dynamical processes within the Atlantic–Africa domain are examined in some detail. The QBZD has a dipole pattern associated with a Walker-type circulation in the near-equatorial zonal plane. It is controlled both by equatorial atmospheric dynamics through a Kelvin wave–like disturbance propagating eastward between its two poles and by land surface processes over Africa, inducing combined fluctuations in surface temperatures, surface pressure, and low-level zonal winds off the coast of West Africa. When convection is at a minimum over central and West Africa, a lack of cloud cover results in higher net shortwave flux at the surface, which increases surface temperatures and lowers surface pressures. This creates an east–west pressure gradient at the latitude of both the ITCZ (10°N) and the Saharan heat low (20°N), leading to an increase in eastward moisture advection inland. The arrival from the Atlantic of the positive pressure signal associated with a Kelvin wave pattern amplifies the low-level westerly wind component and the moisture advection inland, leading to an increase in convective activity over central and West Africa. Then the opposite phase of the dipole develops. Propagation of the QBZD convective envelope and of the associated 200 high-level velocity potential anomalies is detected from the eastern Pacific to the Indian Ocean. When the effect of the Kelvin wave propagation is removed by filtering, the stationary character of the QBZD is highlighted. The impact of the QBZD in combination with a Kelvin wave is illustrated by a case study of the monsoon onset in 1984.

1. Introduction

The central and West African regions depend heavily on rainfall during the summer monsoon season, which corresponds to the northernmost migration of the intertropical convergence zone (ITCZ; Hastenrath 1991). A large amount of work has already been completed on rainfall variability of the African monsoon, through studies on mesoscale convective sys-

tems (MCSs; Laing and Fritsch 1993, 1997; Hodges and Thorncroft 1997; Mathon and Laurent 2001), synoptic-scale easterly waves (Reed et al. 1977; Thompson et al. 1979; Duvel 1990; Thorncroft and Hoskins 1994a,b; Diedhiou et al. 1999; Kiladis et al. 2006; Hall et al. 2006), intraseasonal time-scale variability (Kiladis and Weickmann 1997; Janicot and Sultan 2001; Grodsky and Carton 2001; Sultan et al. 2003; Matthews 2004; Mounier and Janicot 2004; Mounier et al. 2007), and interannual and decadal time scales (Lamb 1978a,b; Nicholson 1978; Newell and Kidson 1984; Folland et al. 1986; Rowell et al. 1995; Ward 1998; Janicot et al. 2001; Rowell 2001; Giannini et al. 2003).

Corresponding author address: Dr. Serge Janicot, LOCEAN/IPSL, Université Pierre et Marie Curie, Boite 100, 4 Place Jussieu, 75252 Paris CEDEX 05, France.
E-mail: serge.janicot@locean-ipsl.upmc.fr

This paper is part of a series of studies addressing the West African summer monsoon dynamics at intraseasonal time scales. Part I (Sultan et al. 2003) highlighted the dominance of 10–25- and 25–60-day periodicities in rainfall and convective activity over the Sahel associated with a westward-propagating signal from eastern Africa to the western tropical Atlantic. Part II (Sultan and Janicot 2003) documented in detail one of the main events on the intraseasonal time scale: the monsoon onset characterized at the end of June by an abrupt northward shift of the ITCZ associated with an enhancement of the Saharan heat low circulation. Mounier and Janicot (2004) extended this work by carrying out an EOF analysis on 10–60-day filtered convection fields during northern summer and showed evidence of two independent modes of convection dominant in the 10–25-day periodicity domain. The first is characterized by a stationary and uniform modulation of convection within the African ITCZ, associated with a modulation of the zonal low-level wind over the equatorial Atlantic and a zonal dipole of convection between Africa and the north equatorial Atlantic off the coast of South America. The second mode is consistent with the signal already detected over the Sahel in Part I (Sultan et al. 2003). In a recent study, Mounier et al. (2007) documented evidence at the synoptic scale of eastward-propagating convectively coupled Kelvin waves within the Atlantic and African ITCZ during northern summer, and quantified their impact on the convective activity in the African monsoon during its onset and full development. They showed in particular that these waves, when present, modulate convection at a similar level as the primary synoptic-scale disturbances within African monsoon system, the so-called easterly waves.

In the present paper, we more thoroughly develop an investigation of the mechanisms leading to the main intraseasonal mode of convection in the African monsoon identified in Mounier and Janicot (2004) that will be called the quasi-biweekly zonal dipole of convection (QBZD). We will also examine its interaction with the synoptic-scale equatorial Kelvin waves and illustrate its impact on the African monsoon through a case study of the 1984 monsoon season, and especially of its onset phase. The second mode, propagating westward over the Sahel latitudes (the “Sahelian” mode; Sultan et al. 2003; Mounier and Janicot 2004), is beyond the scope of this paper and will be examined in future work. This paper is organized as follows: The datasets used in this study are detailed in section 2. Section 3 presents the detection of the QBZD over central and West Africa during northern summer and analyzes its space–time evolution at the regional scale. Some possible mecha-

nisms involved in the dynamics of this mode are examined in section 4. A case study of the 1984 African monsoon season is detailed in section 5. Discussion and conclusions are given in section 6.

2. Datasets

a. *The NCEP–DOE AMIP-II reanalysis*

The National Centers for Environmental Prediction–National Center for Atmospheric Research (NCEP–NCAR) reanalysis dataset (Kalnay et al. 1996) provides a gridded analysis of the global observational network of meteorological variables (wind, temperature, geopotential height, humidity on pressure levels, surface variables) and flux variables such as precipitation rate and radiative and turbulent fluxes. The reanalysis uses a “frozen” state-of-the-art analysis and forecast system at a triangular spectral truncation of T62 to perform data assimilation throughout the period 1948 to present. Data are reported on a $2.5^\circ \times 2.5^\circ$ grid every 6 h (0000, 0600, 1200, and 1800 UTC), on 17 pressure levels from 1000 to 10 hPa as well as the surface level, which are adequate resolutions for studying synoptic weather systems. The NCEP–Department of Energy (DOE) second Atmospheric Model Intercomparison Project (AMIP-II) reanalysis (R-2) dataset, the updated version of the NCEP–NCAR reanalysis, has been used here with one value per day by averaging the four outputs of each day. This version of the reanalysis shows significant improvements over the original, especially for land surface parameters and surface–air fluxes (Kanamitsu et al. 2002).

b. *The NOAA OLR dataset*

Since 1974, launching of polar orbital Television and Infrared Observation Satellite–National Oceanic and Atmospheric Administration (TIROS–NOAA) satellites has established a quasi-complete series of twice-daily outgoing longwave radiation (OLR), at the top of the atmosphere and at a resolution of 2.5° latitude–longitude (Grueber and Krueger 1984). The daily interpolated OLR dataset produced by the Climate Diagnostics Center (Liebmann and Smith 1996) has been used over the period 1979–2000 as a proxy for deep convection. Local hours of the measurements varied during the period 1979–90 between 0230 and 0730 LT in the morning and between 1430 and 1930 LT in the afternoon. Since deep convection over West Africa has a strong diurnal cycle, a sample of daily OLR based on two values separated by 12 h is obtained to get a daily average. Wheeler et al. (2000), Straub and Kiladis (2002), and Roundy and Frank (2004), among oth-

ers, have illustrated the utility of OLR in tracing convectively coupled equatorial waves.

c. The IRD daily rainfall dataset

To validate the OLR data, a daily interpolated in situ rainfall dataset available from Institut de Recherches pour le Développement (IRD) has been used. Daily rainfall amounts at stations located within the West African domain 3° – 20° N, 18° W– 25° E have been compiled. These data are available for the period 1968–90, utilizing more than 1300 stations from 1968 to 1980, and between 700 and 860 for the period 1981–90. These daily values were interpolated to the same $2.5^{\circ} \times 2.5^{\circ}$ grid as NOAA OLR and NCEP fields, by assigning each station daily value to the nearest grid point and averaging all the values related to each grid point. The greatest density of stations is located between the latitudes 5° to 15° N. Data along 17.5° N can also be taken into account since 30 to 45 stations are available near that latitude.

d. The cloud cluster dataset

A database identifying cloud clusters from the full-resolution (30 min , $5 \times 5 \text{ km}^2$) Meteorological Satellite (Meteosat) infrared channel (10.5 – $12.5 \text{ }\mu\text{m}$) has been constructed over the period June–September (JJAS) 1983–99, and MCS identification was carried out through a tracking algorithm based on an areal overlap method (Mathon and Laurent 2001; Mathon et al. 2002). Convective clouds are delineated in Meteosat infrared images using two different brightness temperature thresholds, 233 and 213 K. The 233-K threshold is within the range of the most commonly used thresholds for identifying deep convection (Duvel 1989) and accumulated convective precipitation in the tropics (Arkin 1979). The 213-K threshold targets the most active part of the convective systems. MCSs have been defined as convective clouds larger than 5000 km^2 at the 233-K threshold. With this definition, they contribute to 93% of the total Sahelian cloud coverage at the 233-K threshold for the core of the rainy season July–September (Mathon et al. 2002). MCSs lasting more than 12 h have been retained, and a set of daily duration of MCS occurrences has been constructed on a $1^{\circ} \times 1^{\circ}$ grid. This dataset is available for the monsoon period (June–September) between 1983 and 1999 over the domain 0° – 20° N, 60° W– 40° E. Because of the varying availability of Meteosat data, the extracted areas are not identical, the overlapping area being 5° – 20° N, 20° W– 20° E. No data were available east of 20° E over the period 1989–91, south of 5° N and west of 29° W for the year 1992, and west of 25° W over the period 1993–97.

e. The CLAUS dataset

The European Union funded a project entitled Cloud Archive User Service (CLAUS) to construct an archive of global top-of-the-atmosphere brightness temperature for the period 1983–93. This archive is based on the International Satellite Cloud Climatology Project (ISCCP) level B3 data (Rossow et al. 1997), which are then synthesized to provide a global dataset on a regular 0.5° latitude–longitude grid at 3-hourly intervals, the temporal sampling being sufficient to enable diagnosis of diurnal variability (Hodges et al. 2000; Yang and Slingo 2001). This dataset will be used to illustrate the case study of the 1984 African monsoon season.

3. Detection of the Guinean mode and its regional-scale pattern

a. Local detection

A spatial empirical orthogonal function analysis (SEOF; Richman 1986) has been performed on the 10–90-day bandpass-filtered June–September OLR values over the domain 10° S– 30° N, 30° W– 30° E for the period 1979–2000. The first-mode SEOF1 is presented in Fig. 1. Figure 1a (contours) displays the 10–90-day filtered OLR composite map of strong minus weak convective intraseasonal events, where strong (weak) events are selected when the respective principal component (PC) time series values are maximum (minimum) and greater (lower) than the PC standard deviation. This mode explains 13.3% of the 10–90-day filtered variance and is retained as it passes both the Scree (Cattell 1966) and North (North et al. 1982) tests. SEOF2 is also significant, explaining 7.9% of the variance, but this mode is unrelated to SEOF1 and will not be considered here. It is in fact consistent with the signal detected over the Sahel in Sultan et al. (2003) and will be examined in a follow-on study.

In Fig. 1, SEOF1 represents an enhancement of up to 15 W m^{-2} relative to the mean OLR with higher than 10 W m^{-2} values over the African monsoon domain, since its spatial pattern is superimposed onto the climatological mean of the ITCZ OLR field (in summer the ITCZ is centered along 10° N). To evaluate this result based on OLR as a proxy for convection, composites of unfiltered rainfall fields based on the OLR PC time series have been computed over the period June–September from 1979 to 1990, the common period between the OLR and the IRD-rainfall datasets to examine the correspondence between deep convection and rainfall (Fig. 1a, shaded). This mode is associated with a modulation of rainfall across the entire ITCZ with large differences in precipitation amounts but without

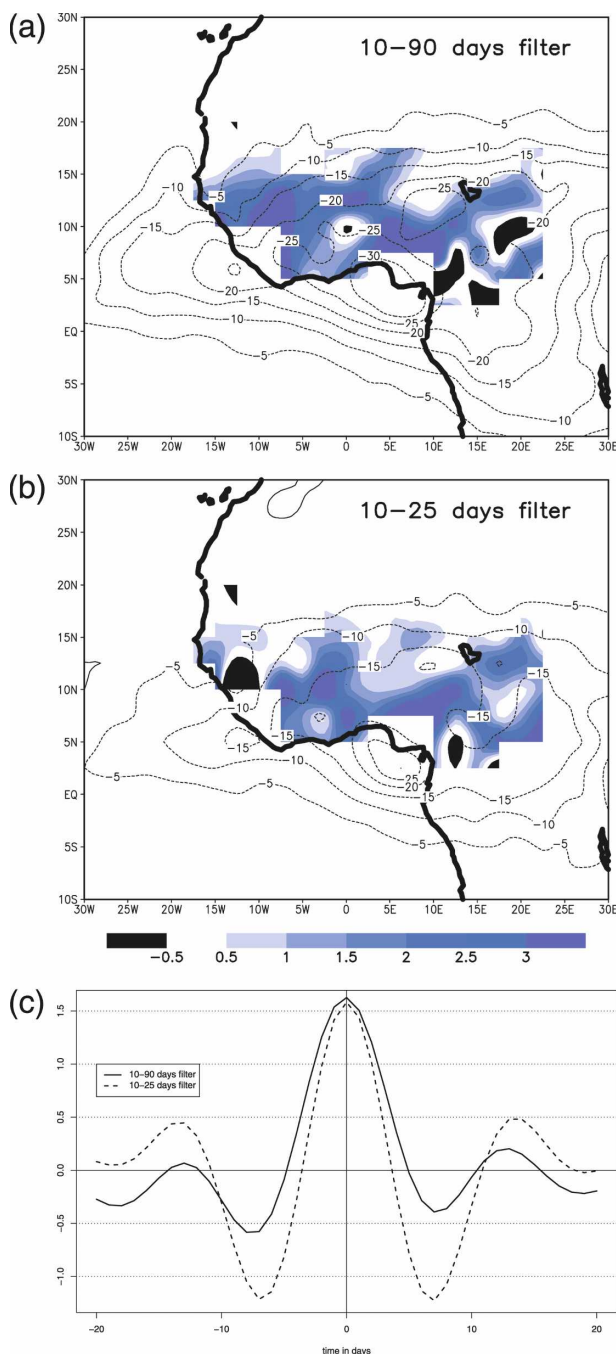


FIG. 1. First mode of an SEOF analysis of 10–90-day filtered OLR values. (a) Composite fields of strong minus weak convective events for JJAS 1979–2000 based on the PC time series (see details in the text); contours, OLR differences ($W m^{-2}$); shaded areas, same as contours but for unfiltered rainfall ($mm day^{-1}$) computed on the period 1979–90. (b) Same as (a) but for SEOF computed on 10–25-day filtered OLR. (c) Normalized composite PC time series of the first EOF mode of filtered OLR over the period band 10–90-day (solid line) and 10–25-day (dashed line), for the difference between strong and weak intraseasonal convective events sequences. This composite sequence is displayed from $t_0 - 20$ days to $t_0 + 20$ days where t_0 is the maximum of the time series.

any significant changes in the latitudinal location of the ITCZ (the highest mean precipitation in the heart of the ITCZ is between 6 and 8 $mm day^{-1}$; see Fig. 6 of Sultan et al. 2003). High positive rainfall anomalies are mainly located where the OLR anomalies are the lowest, especially for the 10–25-day filtered signal (Fig. 1b). However, some qualitative differences appear due to the fact that rainfall data are not filtered at the intraseasonal scale and that there are areas where no rainfall data are available.

Sultan et al. (2003) showed that intraseasonal variability of convection over central and West Africa can be separated into two ranges of periodicities, at less than and greater than approximately 25 days. Figure 1b displays the SEOF1 pattern of OLR but filtered between 10 and 25 days. This pattern explains 10.3% of the filtered variance. It is very similar to the 10–90-day filtered OLR SEOF1 pattern, and in fact dominates the intraseasonal signal. Figure 1c shows the composite PC1 time series for strong minus weak convective event sequence related to the 10–90- (solid line) and 10–25-day (dashed line) filtered OLR SEOF1 modes. It is clear that the 10–90-day mode has a dominant periodicity of 13 days, similar to the mean periodicity of the 10–25-day signal. We also note that away from t_0 the amplitude of the 10–90-day signal is weakened relative to the 10–25-day signal. This results from the contribution of longer periodicity signals mainly belonging to periods between 25 and 90 days (not shown).

Figure 1 shows a much different result than what is obtained when a similar approach is used for 10–90-day OLR including the Indian or west Pacific sectors, where the 30–60-day MJO is the dominant mode (e.g., Knutson and Weickmann 1987). As the 10–25-day signal dominates intraseasonal variability over Africa, we will consider in the following only the 10–25-day filtered OLR SEOF1 mode that we call the QBZD.

The explained variance of this mode is rather weak, so to evaluate its impact on the ITCZ convection area, we have computed the correlations between 10°W and 10°E averaged 10–25-day filtered OLR and their reconstruction by SEOF1 at different latitude bands from the equator to 20°N (Table 1). The high correlation coefficients, up to +0.83 and higher than +0.77 between 2.5° and 12.5°N, emphasize the significance of the SEOF1 mode in explaining intraseasonal variability in the African ITCZ area. A QBZD index has been computed from the reconstruction of the 10–25-day filtered OLR by SEOF1 over the area 2.5°–12.5°N, 10°W–10°E. To better evaluate the contribution of the QBZD in the intraseasonal variability of convection during northern summer, a wavelet analysis (Torrence and Compo 1998) has been performed on indices com-

TABLE 1. Correlation coefficients computed between 10°W and 10°E averaged 10–25-day filtered OLR and their reconstruction by SEOF1 at different latitude bands for the period JJAS 1979–2000.

15°–20°N	0.27
12.5°–17.5°N	0.46
10°–15°N	0.64
7.5°–12.5°N	0.77
5°–10°N	0.83
2.5°–7.5°N	0.80
0°–5°N	0.74

puted over the ITCZ area (2.5° – 12.5°N , 10°W – 10°E) where the correlations with the QBZD are the highest, for the months June to September from 1979 to 2000. Figure 2 displays the mean 1979–2000 wavelet diagrams for the index based on raw OLR (shaded), the index based on OLR reconstructed by the QBZD (dashed contours), and the index based on OLR filtered for the Kelvin wave signal (solid contours) over the period range 2.5–36 days. The Kelvin-filtered OLR values were obtained as in Mounier et al. (2007) by filtering in the wavenumber–frequency domain that included wavenumbers 1–14 and equivalent depth ranging from 8 to 90 m. The raw OLR variability is highest in June and September. Both QBZD and Kelvin-filtered indices also have their peak signals in June; in fact both are highest during spring (not shown) when the convection is located along the Guinean coast at the time of the primary rainy season, and to a lesser extent after mid-September at the time of the second rainy season along the coast. This is consistent with the location of the QBZD pattern and with the fact that convection is more modulated by the dynamics of equatorial Kelvin waves when the ITCZ is closer to the equator. It is also clear that activity of both QBZD and Kelvin waves contribute substantially to the overall OLR variability during summer. The QBZD activity is centered between 12 and 15 days but extends over a wider period domain covering the whole 10–25-day range. We also note that while Kelvin waves are more active at synoptic time scales (the main Kelvin mode has been shown to operate at a 6-day periodicity; Mounier et al. 2007), very little Kelvin variability is present at periods higher than 10 days to superimpose onto the QBZD signal.

b. Regional-scale space–time evolution of the QBZD

We focus now on atmospheric composite fields based on the QBZD index. As this index is expressed through OLR values, a maximum in the corresponding time series means weaker convection. We retained the dates t_0

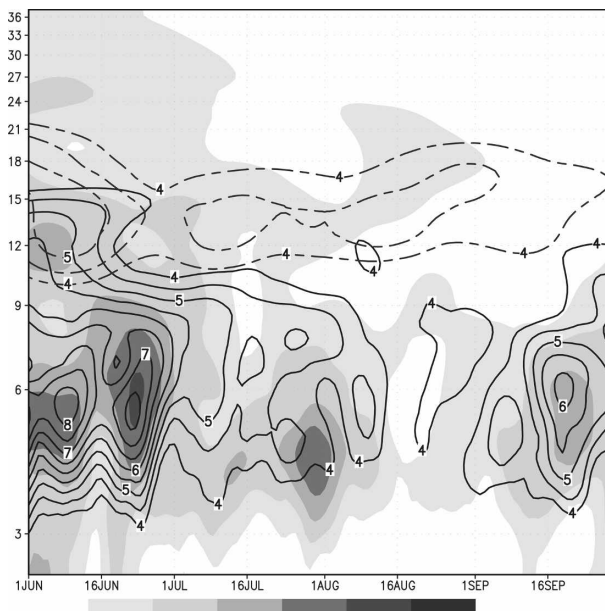


FIG. 2. Mean wavelet diagram performed for indices computed over the ITCZ area (2.5° – 12.5°N , 10°W – 10°E) for the months June to September averaged over 1979–2000. Shaded areas, indices based on raw OLR; dashed contours, indices based on OLR reconstructed by the QBZD; solid contours, indices based on OLR filtered for the Kelvin wave signal. The diagram is presented over a period range of 2.5–36 days.

where this index is maximum (minimum) and the deviation from its mean for each year is greater (lower) than its standard deviation to define a weak (strong) convective phase of the QBZD.

Figure 3 shows the strong minus weak convective composite sequence associated with this QBZD index for the 10–25-day filtered OLR and the unfiltered 200-hPa velocity potential fields. OLR and velocity potential values are displayed when significant at the 90% level. These sequences go from t_0 minus 6 days to t_0 plus 6 days with an irregular lag. Between five and six cases per summer have been retained for strong and for weak convective phases. The first character of the QBZD sequence to note is a modulation in convection as a standing oscillation growing and decreasing over the southern coast of West Africa and over central Africa. Moreover, an opposite polarity is centered at 40°W , yielding evidence of a zonal dipole. This time sequence also confirms that the dominant periodicity of these fluctuations is at intraseasonal time scales, between 12 and 13 days as seen in Fig. 1c, since we get a rather similar OLR anomaly field at $t_0 - 6$ and $t_0 + 6$ but with a smaller eastern lag on $t_0 - 6$ (this periodicity will be also confirmed in Fig. 7).

A second characteristic of this sequence concerns the eastward propagation of OLR anomalies over the

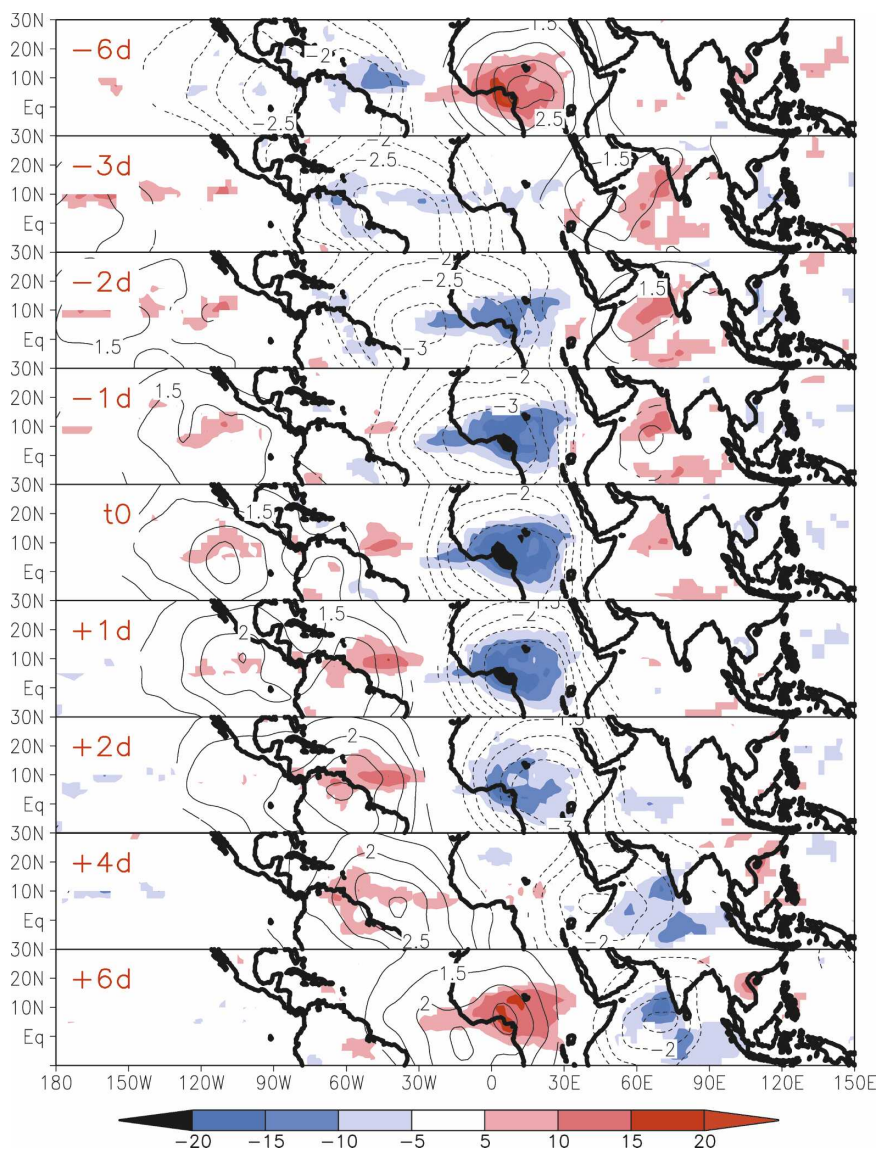


FIG. 3. (top to bottom) Composite time sequences based on the QBZD index. Dates (t_0) where this index is maximum (minimum) and its deviation from its mean is greater (lower) than 1 std dev have been retained to define a weak (strong) convective phase of the QBZD. The respective strong minus weak convective composite sequences are shown for the 10–25-day filtered OLR (W m^{-2} , shaded) and unfiltered 200-hPa velocity potential ($10^6 \text{ m}^2 \text{ s}^{-2}$, contours) fields. This sequence goes from $t_0 - 6$ days to $t_0 + 6$ days with irregular lags (days are marked in the left upper corners). OLR and velocity potential values are displayed when significant at the 90% level.

equatorial Atlantic between the two poles of convection. A third point is that this signal continues propagating eastward to modulate convection over the Indian Ocean. There is not a clear propagation of the negative OLR anomalies from central Africa to the Indian basin: the signal of OLR enhancement remains stationary from $t_0 - 2$ to $t_0 + 2$ over Africa, then abruptly disappears at $t_0 + 3$ while reappearing over the Indian

Ocean. This may be due to the East African orography that separates the convective regime over East Africa where MCSs initiate and move westward from the Indian sector convective regime belonging to the Indian monsoon system. However, the unfiltered 200-hPa velocity potential field sequence, closely linked to the OLR filtered fields, highlights the propagating character of the upper-level dynamical signal across the East

African mountains. A final point is that the propagation of OLR anomalies and of the associated 200-hPa velocity potential patterns is also evident over the eastern Pacific whereas the signal is weaker than over the Indian Ocean. From this we conclude that the QBZD is embedded in a regional-scale pattern over a domain larger than Africa itself, and in fact it may be related to a global-scale pattern linked to variability over the Amazon and Pacific studied by Chen et al. (2001) and Chelliah and Bell (2004). In these studies pattern having components of the QBZD emerge in a global analysis of interannual to multidecadal variability.

Although synoptic-scale disturbances as well as meso-scale convective systems over Africa and the tropical Atlantic generally travel westward, eastward propagation of convective signals in the African monsoon have recently been documented (Mounier et al. 2007; Mekonnen et al. 2006; Wang and Fu 2006). It has been shown that Kelvin waves significantly modulate the convective intensity over this area through an eastward displacement of a “convective envelope,” as seen both through the OLR data and the high-resolution cloud cluster dataset. Similar computations have been performed here using the high-resolution cloud cluster data. These data are rather consistent with the OLR data since they are both based on satellite irradiance but some differences exist due to the sampling, which is greatly enhanced for the MCS dataset. Strong minus weak convective composite sequences of MCS occurrences based on the QBZD index are shown in Fig. 4 for the period June–September 1983–99. Only MCSs lasting more than 12 h have been considered; these MCSs have a larger mean size (Fig. 6 of Mathon and Laurent 2001). These MCSs contribute to about 75% of their total coverage at the 233-K threshold, which demonstrates the importance of long-lived MCSs in spite of their small occurrence numbers (Fig. 6 of Mathon and Laurent 2001). MCS occurrence is expressed on each grid point as duration of occurrences per day by 30-min steps (the scale can go then from 0 to 48; the mean

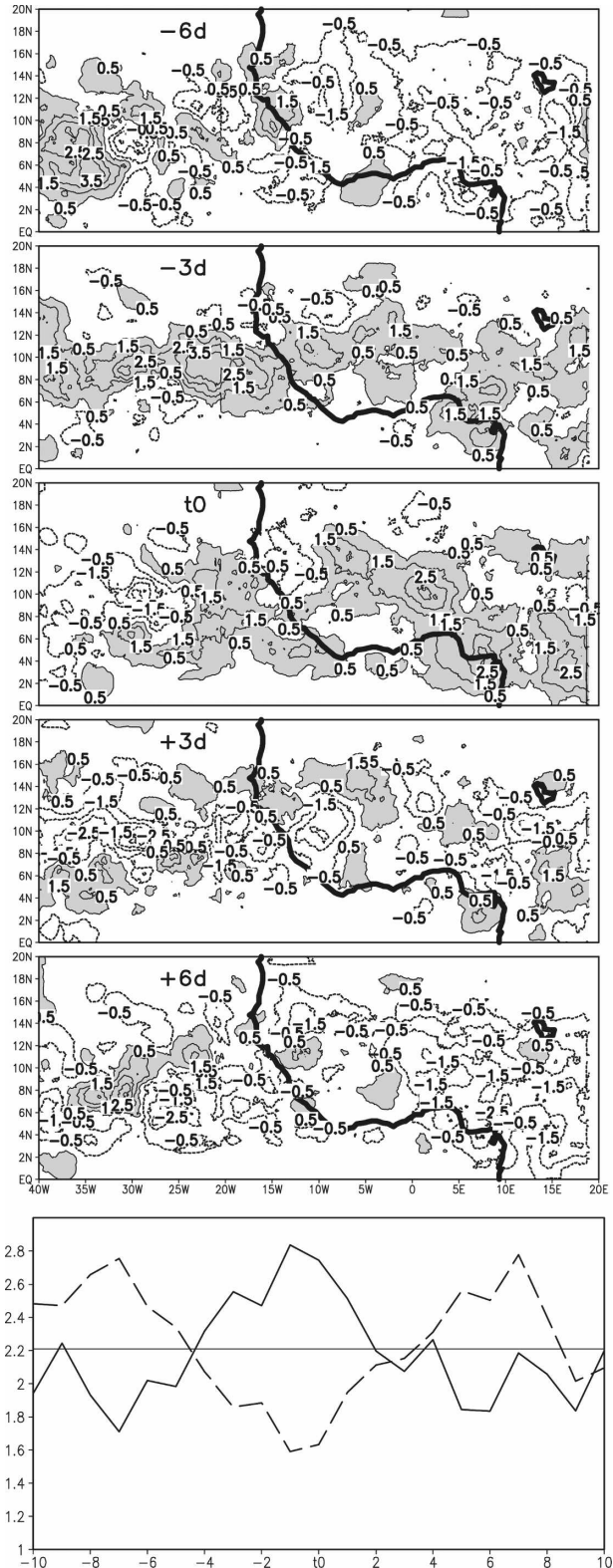


FIG. 4. Same as in Fig. 3, but for MCS occurrences at the 233-K threshold for the period June–September 1983–99. The MCS dataset is available over the domain 0°–20°N, 40°W–20°E. MCS occurrence is expressed as the duration of occurrences per day in 30-min steps (the scale can then go from 0 to 48) for MCSs lasting more than 12 h (shaded for positive values). The time sequence goes from $t_0 - 6$ days to $t_0 + 6$ days with a 3-day lag. (bottom) The corresponding composite time series from $t_0 - 10$ to $t_0 + 10$ days of the mean MCS occurrences averaged over the area 2.5°–12.5°N, 10°W–10°E for strong (solid line) and weak (dashed line) convective intraseasonal events. The horizontal line represents the overall mean. The African coastline is shown as the heavy line.

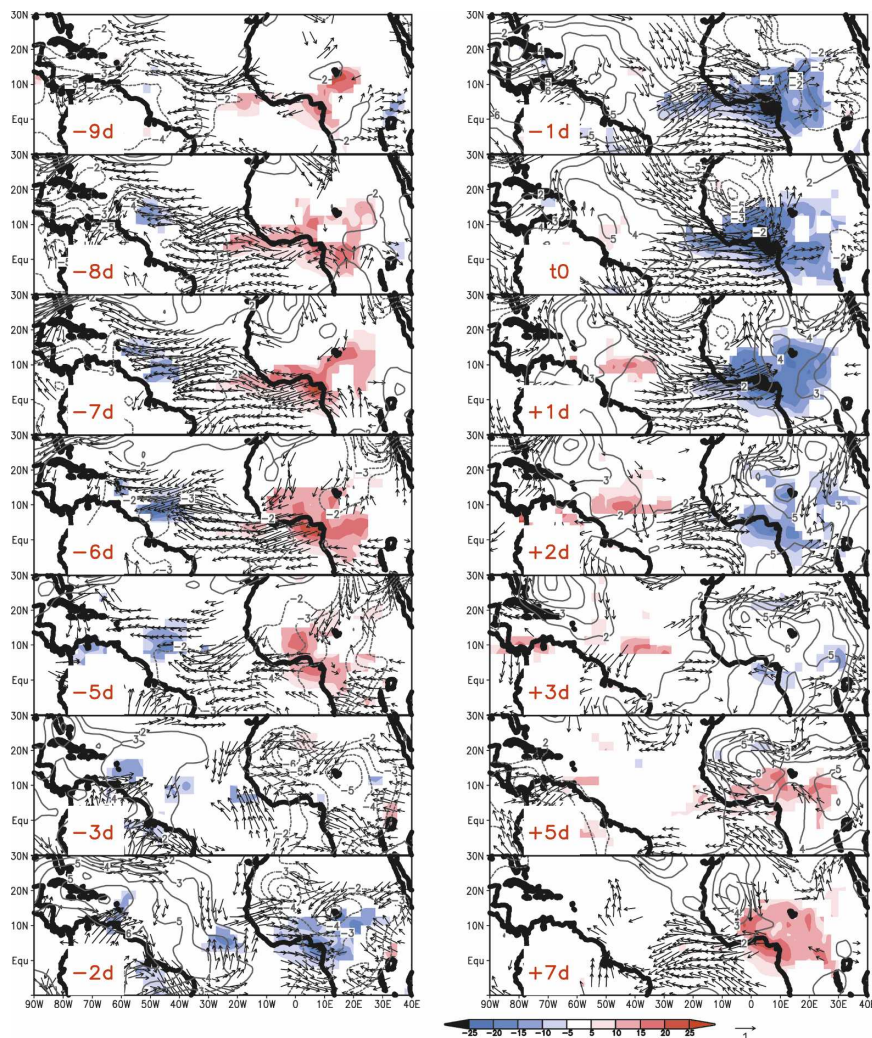


FIG. 5. Same as in Fig. 3, but for unfiltered OLR (W m^{-2} , shaded), wind (vectors, scale in m s^{-1} displayed beneath the panels), and geopotential height (gpm, contours) at 925 hPa. (top to bottom) This sequence goes from $t_0 - 9$ days to $t_0 + 7$ days with irregular lags (days are marked in the left lower corners). The values are displayed when significant at the 90% level.

value in the African ITCZ is approximately 3). These results show the eastward-propagating envelope of the QBZD signal modulating the mean duration of occurrences of MCSs from the eastern tropical Atlantic to central and West Africa, and in particular over the Fouta Jalon and Cameroon highlands. This can induce breaks over the entire extent of the ITCZ convective belt due to its large zonal extension (not shown). The time series at the bottom of Fig. 4 represents the corresponding composite time series from $t_0 - 10$ to $t_0 + 10$ days of the mean MCS occurrences averaged over the area $2.5^\circ\text{--}12.5^\circ\text{N}$, $10^\circ\text{W--}10^\circ\text{E}$ for strong (solid line) and weak (dashed line) convective intra-seasonal events. It shows the highly symmetric charac-

ter of the modulation of the convective activity and confirms a mean periodicity of about 14 days. The amplitude of the modulation is also high relative to the mean (the horizontal line) with a percentage of about 30% at t_0 to $t_0 - 1$.

4. QBZD dynamical structure

We focus now on the Atlantic–African domain to further investigate the dynamical structure of the QBZD. Composite sequences of strong minus weak convective QBZD phases for unfiltered OLR and atmospheric fields will be considered (Figs. 5–8). The objective is to gain insight into the dynamics of the dipole

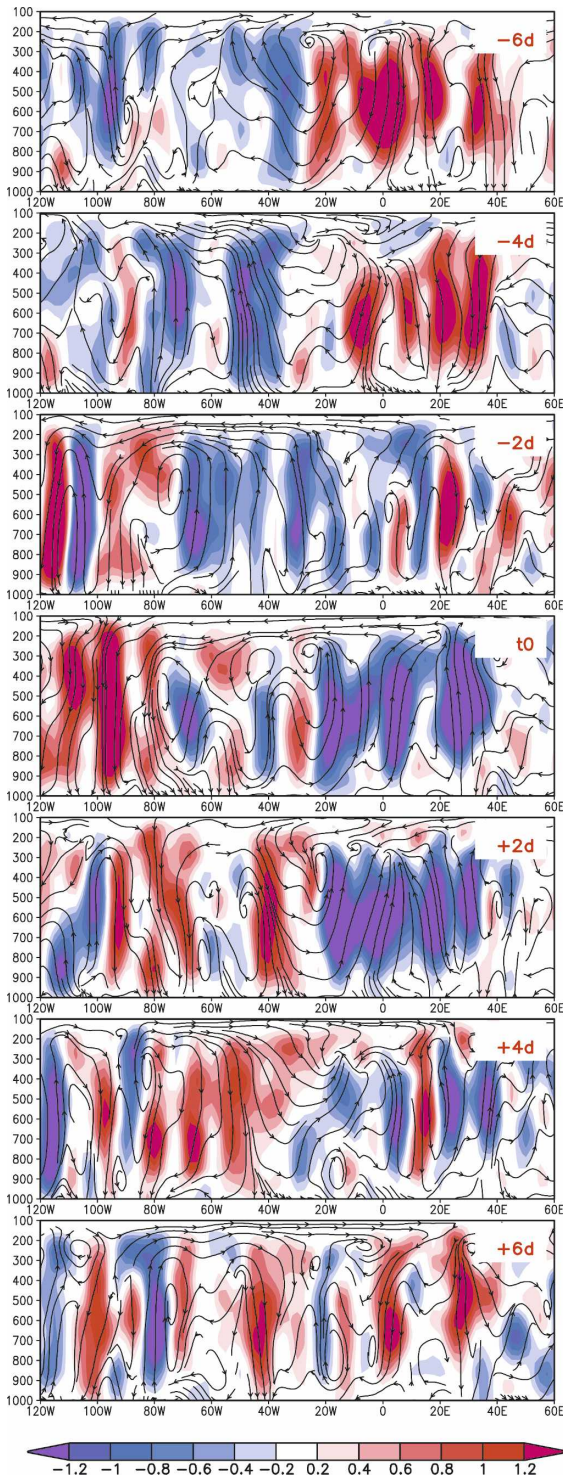


FIG. 6. Same as in Fig. 3, but for longitude–pressure cross section of unfiltered vertical motion (shaded, $\text{Pa s}^{-1} \times 50$) and streamlines of unfiltered zonal circulation. Values are averaged on the latitude band 2.5° – 12.5°N . (top to bottom) The sequence goes from $t_0 - 6$ days to $t_0 + 6$ days with a 2-day lag (days are marked in the right upper corners).

pattern associated with the QBZD and its mixed stationary–propagating character. The horizontal pattern will be analyzed through a time sequence of OLR, NCEP wind, and geopotential height at 925 hPa (Fig. 5). The vertical structure will be analyzed in Fig. 6 through a time sequence of vertical circulation along a longitudinal axis (averaged over 2.5° – 12.5°N latitude).

The summer atmospheric circulation in a meridional plane over West Africa does not yield the traditional view of a meridional Hadley-type circulation. It is in fact largely disturbed by the predominance of the heat low transverse circulation between the surface and 500 hPa (see, e.g., Fig. 8 of Sultan and Janicot 2003). This circulation is well developed with a dry convective area around 20°N and subsidence between 25° – 30°N and between 10° – 15°N . This circulation interacts both with the northern subsiding branch of the Hadley-type cell north of 20°N and with the ascending branch of the ITCZ around 10°N . The heat low transverse circulation not only disturbs the northern Hadley-type circulation but also distorts the meridional circulation of the southern Hadley-type cell by influencing the northern extension of the low-level southerly monsoon winds up to 20°N . The heat low also affects the zonal circulation of the lower half of the troposphere, especially the cyclonic circulation of the low-pressure center controlling the westerly component of the monsoon winds.

Time series of standardized indices have also been defined by averaging selected NCEP variables (observed OLR, NCEP vertical velocity at different pressure levels, surface temperature, mean sea level pressure, cloud cover and net surface short wave budget, 925- and 200-hPa zonal wind) over three key zones (Fig. 7): the Saharan heat low area (Z1; 15° – 20°N , 15°W – 10°E) characterized by dry convection in the low levels below 500 hPa and overlain by subsiding air of the northern Hadley-type circulation over Africa; the eastern pole area of the QBZD over Africa (Z2; 2.5° – 12.5°N , 20°W – 20°E); and the western pole area of the QBZD over the Atlantic (Z3; 2.5° – 12.5°N , 55° – 30°W). Other indices defined over other nearby areas have also been used and will be described when necessary. The analysis of the links between the modulation of convection in the African ITCZ and low-level moisture advection will be based on the NCEP 925-hPa wind and 400-hPa vertical velocity data. We have confirmed that at low levels moisture transport is highly correlated to the wind field itself, as has been very often shown in other studies. To limit the number of indices used, we have also preferred to use 400-hPa vertical velocity rather than low-level moisture convergence because convection in Africa does not depend only on moisture convergence but also on local instability, so that indices

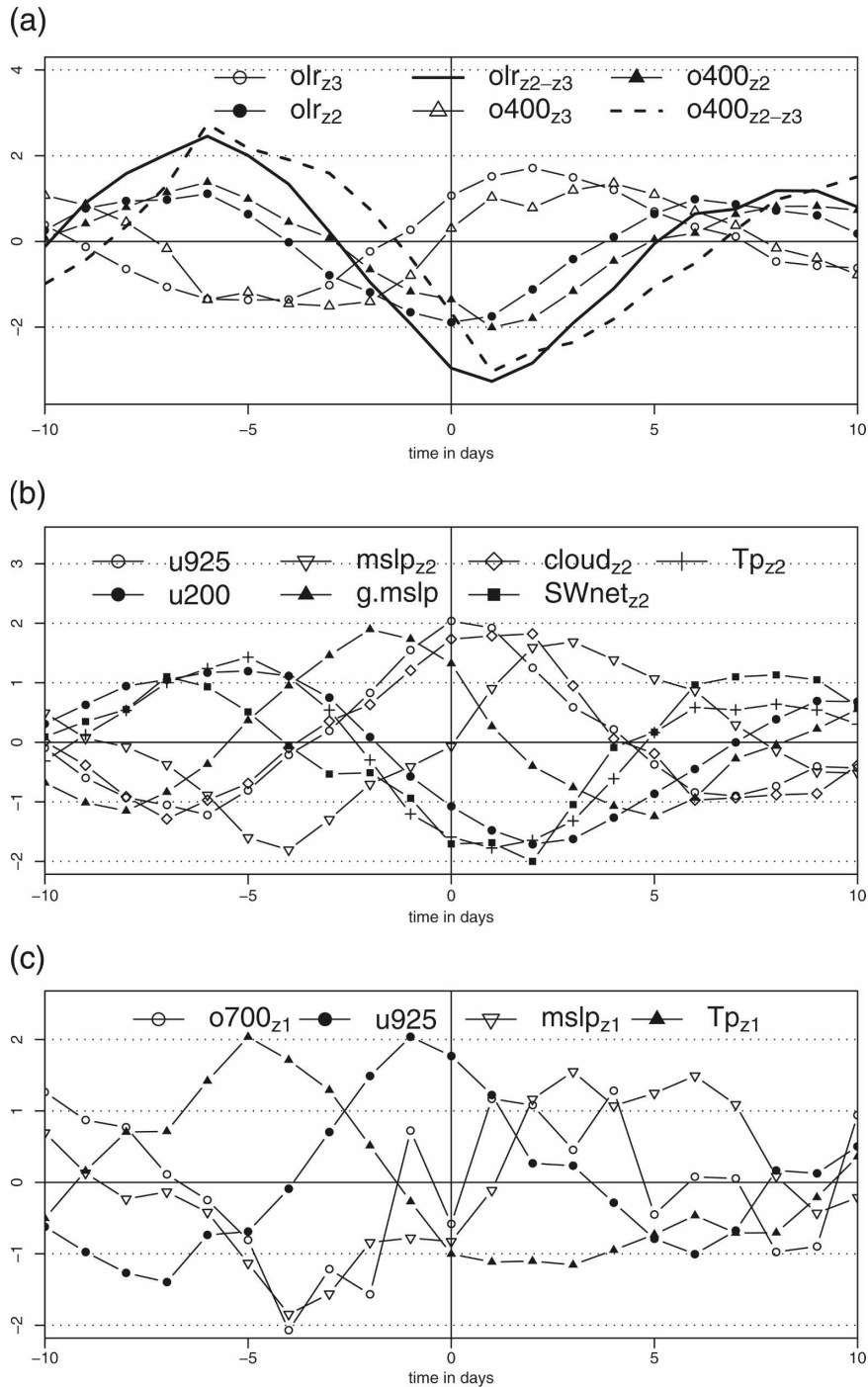


FIG. 7. Composite time series based on the QBSD index as in Fig. 3, but for time series of standardized unfiltered indices from $t_0 - 10$ days to $t_0 + 10$ days (see text for more details). (a) OLR and 400-hPa vertical velocity in areas Z2 and Z3: OLR_{Z2} , OLR_{Z3} , OLR_{Z2-Z3} , $o400_{Z2}$, $o400_{Z3}$, $o400_{Z2-Z3}$. (b) Surface temperature (Tp_{Z2}), mean sea level pressure ($mslp_{Z2}$), cloud cover ($cloud_{Z2}$), and net surface short wave budget ($SWnet_{Z2}$) on area Z2, 925-hPa zonal wind on the area 0° – 10° N, 35° W– 0° ($u925$), 200-hPa zonal wind on the area 15° S– 10° N, 40° W– 20° E ($u200$), mean sea level pressure difference between 0° – 10° N, 60° – 30° W and 0° – 10° N, 10° W– 40° E ($g.mslp$). (c) 700-hPa vertical velocity ($o700_{Z1}$), surface temperature (Tp_{Z1}), and mean sea level pressure ($mslp_{Z1}$) on area Z1, and 925-hPa zonal wind on the area 10° – 20° N, 25° W– 0° ($u925$).

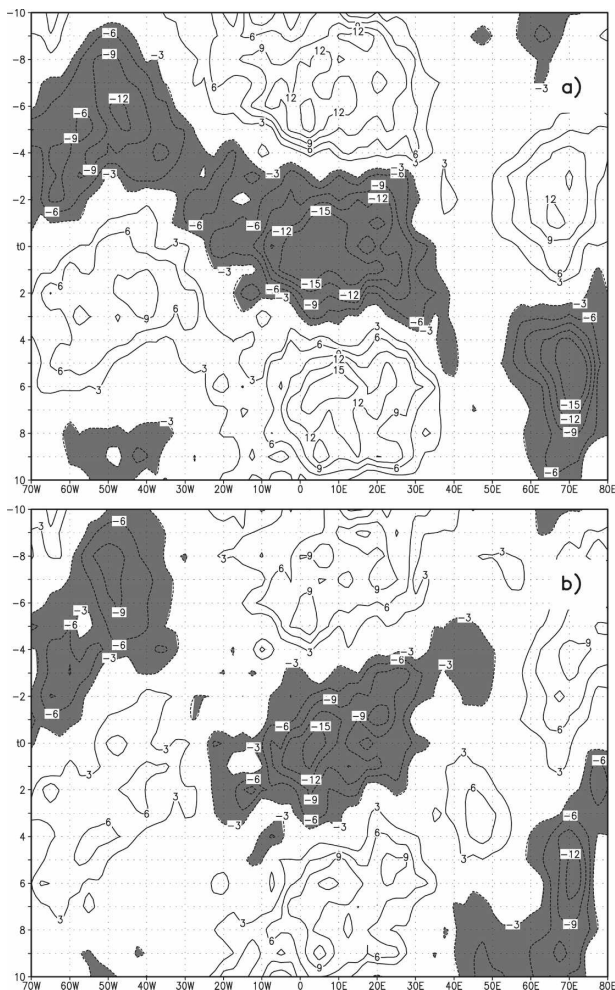


FIG. 8. Mean composite time-longitude diagrams averaged over 2.5° – 12.5° N of unfiltered OLR for (a) the QBZD and (b) the QBZD where the Kelvin wave signal has been removed (see details in the text). Negative values are shaded.

like convective available potential energy (CAPE) and convective inhibition (CIN) are also important. However we have verified that the sequence of spatial patterns of moisture convergence over central and West Africa is consistent with the evolution of the other variables (not shown).

We first consider the zonal convection dipole evolution through a composite time series of the OLR indices (Fig. 7a). OLR_{Z2} shows a 12-day periodic signal as was seen in Fig. 3. By definition OLR_{Z2} has its lowest value at t_0 when convection is the highest over West Africa, and it has its highest value six days before when convection is weakest. OLR_{Z3} over the western pole of the QBZD dipole shows a clear out-of-phase evolution with OLR_{Z2} , however with a slight lag of one to two days (Fig. 7a). This means that, as seen in Fig. 3, OLR_{Z3} reaches its weakest (highest) value one or two days

after OLR_{Z2} reaches its highest (weakest) value. The standardized dipole index OLR_{Z2-Z3} shows a slightly longer periodicity of about 14 days with its lowest value at $t_0 + 1$ (Fig. 7a). Vertical velocity indices at 400 hPa ($\omega_{400_{Z2}}$ and $\omega_{400_{Z3}}$; negative values for upward motions) are highly consistent with associated OLR indices, except they reach their extrema about one day after OLR indices (Fig. 7a). Some interpretation of the dynamics of the QBZD dipole are now given by considering its step-by-step evolution, beginning around $t_0 - 6$ when convection is weakest over West Africa and at its strongest over its western pole (recall that Figs. 5–7 are expressed as mean composite differences between strong and weak convective events over central and West Africa).

a. From $t_0 - 9$ to $t_0 - 4$

At 925 hPa (Fig. 5) a negative pole of geopotential high anomalies develops over the domain 80° – 20° W, 10° S– 15° N at $t_0 - 9$ to $t_0 - 8$, being rather symmetric about the equator. At this time, the large-scale zonal mean sea level pressure (MSLP) difference between 60° – 30° W and 10° W– 40° E reaches its highest negative values (Fig. 7b). From $t_0 - 7$ to $t_0 - 4$, this negative pole travels rapidly eastward and settles over Africa (Fig. 5) where MSLP reach their lowest values at $t_0 - 4$ (Fig. 7b). At $t_0 - 6$ when the QBZD OLR dipole index is the highest and convection over Africa the weakest, the zonal wind component at 925 hPa over the area 0° – 10° N, 35° W– 0° shows consistent behavior by reaching its highest easterly value (Fig. 7b), meaning that less moisture is advected inland. Consistent with the OLR pattern, Fig. 6 depicts at this time a Walker-type circulation in a near-equatorial plane linking downward motions over 20° W– 40° E with upward motions over 50° – 30° W. Within this circulation the 925-hPa zonal wind is in phase with the OLR_{Z2} convective pole over Africa, and 200-hPa zonal winds reach their highest westerly values one day later at $t_0 - 5$ as convection is strongest over Z3 as shown by OLR and strongest at $t_0 - 3$ in the 400-hPa vertical velocity index (Figs. 7a,b). These horizontal and vertical QBZD atmospheric patterns, as well as the rapid eastward propagation over the Atlantic between $t_0 - 7$ and $t_0 - 4$, are very similar to the structure and behavior of the convectively coupled Kelvin waves detected over these regions by Mounier et al. (2007), although the periodicity is very different, between 12 and 14 days for the QBZD instead of 6 days for the Kelvin wave. In Mounier et al. (2007) we showed that these waves interact strongly with convection in the ITCZ and are centered a bit north of the equator symmetrically around 5° N.

We saw that the low-level zonal wind over the equatorial Atlantic is consistent with the QBZD dipole evolution by reaching its highest values at $t_0 - 6$. However, the persistence of weak convection over Africa is associated with reduced cloud cover and higher net shortwave flux at the surface (Fig. 7b), which leads to high surface temperatures over the Z2 area at $t_0 - 5$ (Fig. 7b) and the lowest MSLP at $t_0 - 4$ as seen above (Fig. 7b). So following $t_0 - 6$, the combination of the eastward propagation of low pressure toward Africa and the development of low pressure over Africa due to less cloud cover and convection appears to contribute to the reversal of the zonal wind component over the equatorial Atlantic, which reaches its highest westerly value at t_0 (Fig. 7b).

The convection and cloud cover decrease over Africa contributes to a temperature increase there (Z2) and also northward and especially over the area of the Saharan heat low location (Z1). Figure 7c shows that over the area Z1 the temperature is highest at $t_0 - 5$, followed by maximum upward motions at 700 hPa and minimum MSLP at $t_0 - 4$.

b. From $t_0 - 4$ to $t_0 + 2$

The enhancement of the Saharan heat low activity around $t_0 - 4$ leads to an increase of westerly winds at 925 hPa on the area $10^\circ\text{--}20^\circ\text{N}$, $25^\circ\text{W--}0^\circ$ (whose index reaches its highest value at $t_0 - 1$; see Fig. 7c) associated to a slow westward development of the heat low cyclonic circulation. This signal combined with lower pressures over Africa due to the cloud cover decrease, and the temperature increase began contributing to an increase of inland moisture advection (see Fig. 5 at $t_0 - 3$). This process is accelerated by the arrival of the leading edge of the positive 925-hPa geopotential pole of the Kelvin-type wave pattern from the west after $t_0 - 2$ (Fig. 5), which then leads to the highest westerly winds around t_0 from the equator to 20°N (Fig. 5 and 7b,c) and the highest convective activity over Africa at t_0 . The Walker-type circulation of the previous phase (around $t_0 - 6$) moves eastward and an opposite Walker-type circulation develops over Africa and the Atlantic between t_0 and $t_0 + 2$ with a similar two-day time lag between first peak in convection and 925-hPa westerly wind over Z2, and the 200-hPa easterly wind and lower convection over Z3 (Figs. 7a,b). In the meridional plane over West Africa, upward motion in the ITCZ is highly enhanced whereas dry convection decreases in the Saharan heat low.

c. From $t_0 + 2$ to $t_0 + 7$

At this point the opposite phase of the QBZD dipole is developing. Westerly moisture advection decreases in

Africa due to both the westward propagation and vanishing of the cyclonic circulation in the Saharan heat low as well as the eastward propagation of the Kelvin-type wave pattern at the latitude of the ITCZ (Fig. 5). This is also combined with pressure rise over Africa due to the arrival of the Kelvin-type positive 925-hPa geopotential pole from the west and due to higher cloud cover over Africa inducing lower surface temperatures, leading to higher pressures at $t_0 + 3$ (Fig. 7b). In the near-equatorial zonal plane this is accompanied by an eastward propagation of the Walker-type circulation and the development of an opposite phase over Africa and the Atlantic (Fig. 6). In the meridional plane over West Africa, lower surface temperatures between t_0 and $t_0 + 4$ in the Saharan heat low area (Z1) lead to subsiding anomalous motions (Fig. 7c), consistent with the development of an anticyclonic circulation and easterly winds along the coast of West Africa (see at $t_0 + 5$ in Fig. 5). The combined effect is to lead to a reversal of the large-scale zonal MSLP difference between $60^\circ\text{--}30^\circ\text{W}$ and $10^\circ\text{W--}40^\circ\text{E}$ ($t_0 + 5$; Fig. 7b), inducing a reversal of the low-level zonal winds, which reach their highest easterly values at $t_0 + 7$ (Fig. 7b). Convection over Africa (Z2) then decreases up to $t_0 + 6$, as well as cloud cover, so that surface temperature can increase again due to a net surface shortwave flux enhancement (Fig. 7b). A new cycle of the QBZD dynamics can then begin.

d. Interactions between the QBZD and equatorial Kelvin waves

The QBZD dynamical structure identified here shows a high degree of similarity with the biweekly oscillation detected by Grodsky and Carton (2001) during spring 2000 by using Quick Scatterometer (QuikSCAT) wind and Tropical Rainfall Measuring Mission (TRMM) rainfall data. They demonstrated evidence of a similar mechanism based on the coupling between convective modulation over Africa and related land surface temperature and zonal surface pressure gradient anomalies, leading to variations in the zonal wind field over the eastern Atlantic. However, apart from the fact that we are studying northern summer 1979–2000 while they looked at only spring 2000, some other differences emerge between their analysis and ours. First, they describe a stationary mode controlled mainly by convection and the surface radiation budget over Africa, whereas the QBZD highlights a zonal convection dipole in which eastward propagation over the Atlantic is dominant through Kelvin-type wave dynamics. Second, we infer the role of the Saharan heat low north of the ITCZ in developing a low-level cyclonic circulation when surface temperatures are

higher, leading to an increase of moisture advection inland. The implication of the heat low center of action helps us in understanding why the detected signals can be significant rather far from the equator, whereas Kelvin waves are more closely developed around a 5°N zonal axis (see Mounier et al. 2007). At this time we assume that the QBZD dynamics we analyze over 22 northern summers is a statistical rendition of the case study of Grodsky and Carton, whose structure is embedded in a larger zonal convection dipole and whose internal dynamics is probably linked to Kelvin wave propagation. The QBZD then comprises a sequence involving a stationary phase of convection between $t_0 - 8$ and $t_0 - 6$, a transition phase of internal eastward propagation between $t_0 - 4$ and $t_0 - 2$, another stationary phase of opposite sign between $t_0 - 2$ and $t_0 + 2$, another transition phase between $t_0 + 2$ and $t_0 + 4$, and a stationary phase between $t_0 + 4$ and $t_0 + 8$ similar to the first one.

To explore the possible effect of the Kelvin wave dynamics within the QBZD zonal dipole, we removed from the QBZD reconstruction the Kelvin-filtered OLR signal represented by the box in the wavenumber–frequency domain that included wavenumbers 1–14 and equivalent depth ranging from 8 to 90 m (see Fig. 1 in Mounier et al. 2007; this corresponds to periods between 2.5 and 20 days with highest signals over Africa between 4 and 9 days and a maximum around 6 days as seen in Fig. 2), and compared this result with the full QBZD pattern. This analysis is done by computing composite longitude–time diagrams of OLR related to the occurrences of the QBZD with and without the Kelvin wave signal. It should be noted that removal of the Kelvin variability still leaves the bulk of the variance in eastward-propagating OLR.

Figure 8 shows the mean strong minus weak convective composite time–longitude diagrams for averaged 2.5°–12.5°N unfiltered OLR for (a) the QBZD (constructed as in section 3) and (b) the QBZD when the Kelvin wave signal is removed from the unfiltered OLR. The diagram for the full QBZD (Fig. 8a) depicts the stationary biweekly modulation of convection over central and West Africa followed by a 2-day lag for the occurrence of the opposite-sign western pole around 40°W. Eastward propagation of the convection signal from 70°W to 40°E is also evident, while no clear propagation appears in the OLR field over the Indian Ocean, where a new negative OLR pole is present at 70°E. When the Kelvin wave signal is removed (Fig. 8b), the stationary character of the QBZD dipole is highlighted and the propagating signal over the tropical Atlantic is completely suppressed. This demonstrates

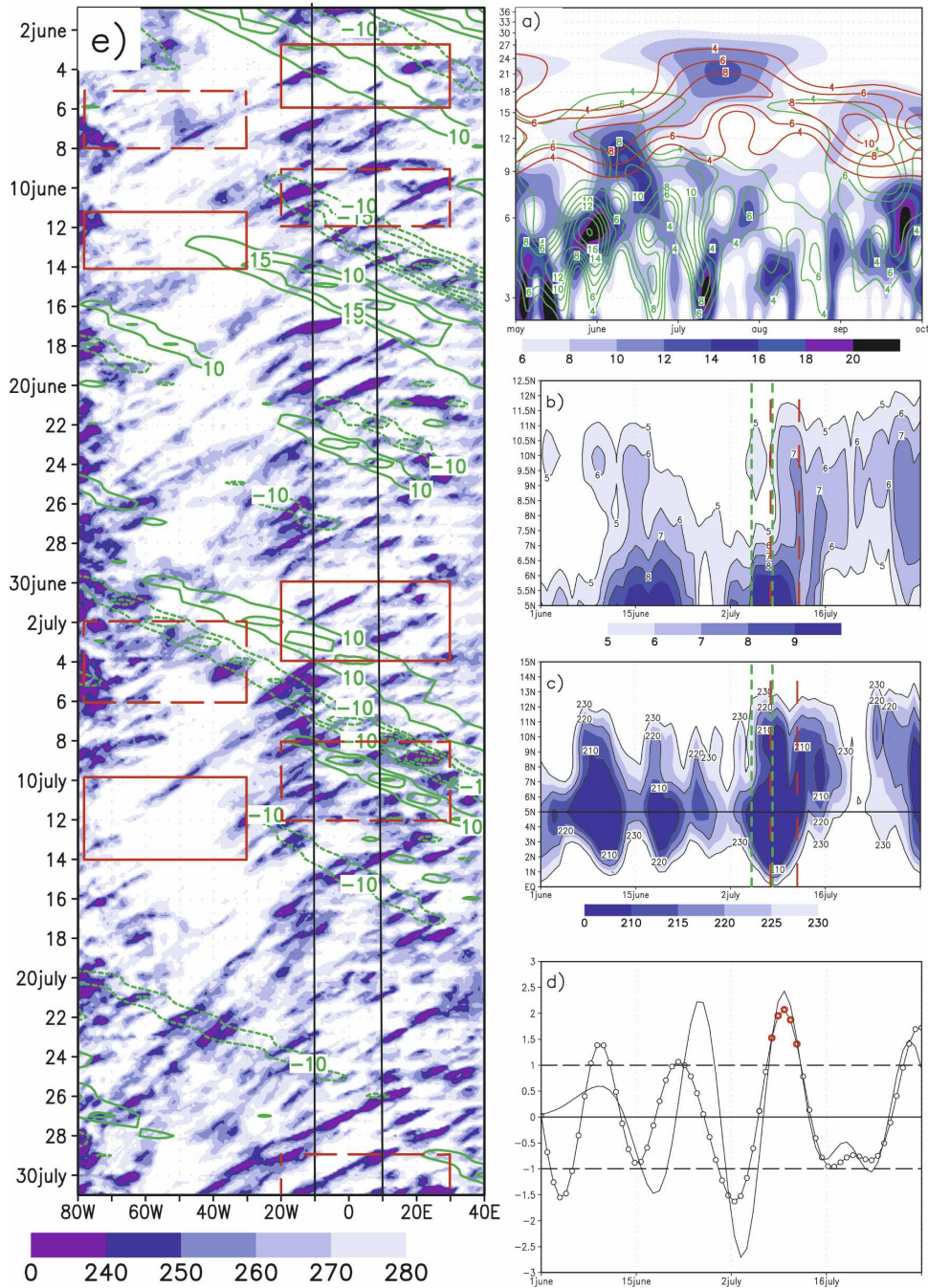
statistically that the QBZD is composed both by a stationary dipole with strong interactions with surface processes, as was initially shown by Grodsky and Carton (2001), and by Kelvin wave dynamics linking the western pole of the QBZD to its eastern pole of the same sign with a time lag of about 5 days.

5. Case study of the 1984 African monsoon season

The objective in this section is to show, through study of the summer monsoon of 1984, evidence of the impact of the QBZD on the convection variability over central and west Africa and to illustrate an example of the combination of the QBZD with a Kelvin wave at the time of the monsoon onset. Over West Africa, the onset stage of the monsoon is characterized by an abrupt latitudinal shift of the ITCZ from a quasi-stationary location at 5°N in May–June to another quasi-stationary location at 10°N in July–August (Sultan and Janicot 2000, 2003; Le Barbé et al. 2002). The mean date for the onset occurrence is 24 June and its standard deviation is 8 days (Sultan and Janicot 2003). This abrupt shift occurs mostly between 10°W and 5°E, where a meridional land–sea contrast exists, and it is characterized by a temporary rainfall and a decrease in convection over West Africa.

Figure 9 shows various plots of the 1984 African monsoon season. Sultan and Janicot (2003) defined the monsoon onset date to be on 3 July during this year based on IRD rainfall indices at 5° and 10°N. It can be seen on the time–latitude diagrams of IRD rainfall and OLR (Figs. 9b,c) that this date corresponds to the beginning of the transition phase leading to the onset of rainfall at the northernmost latitudes, also characterized by the abrupt displacement of the ITCZ from the Guinean Coast to the Sahelian latitudes. The year 1984 was very unusual for the African summer monsoon season since it was the driest recorded during the last century. This was hypothesized to be due to highly abnormal warm sea surface temperatures in the Guinea Gulf leading to an abnormal southward location of the ITCZ during summer (Lamb et al. 1986). For instance, the ITCZ axis was located about 9°N in the latter part of July 1984 instead of the usual 11°N in the multiyear mean (Le Barbé et al. 2002), and the 5 mm day⁻¹ isoline only reached 12°N instead of 14°N, typical for the mean (Sultan and Janicot 2003). This fact may have been favorable to an enhancement of interactions between the ITCZ and equatorial Kelvin waves, since the ITCZ was nearer to the equator.

Figure 9a shows a wavelet diagram similar to Fig. 2 but for the period May–September 1984. High activity in the QBZD is shown (red contours) having a mean



periodicity of 12 days during spring and fall, transitioning to near 20 days in July, with a statistical significance level higher than 90% (not shown). The QBZD evolution is consistent with the variability of the unfiltered OLR signal (shaded). Figure 9d shows a time series of the QBZD index (open circles). It is easily seen that positive (negative) sequences of the QBZD coincide with similar enhanced (weakened) sequences of convection in the ITCZ (Fig. 9c), confirming the dominant

impact of the QBZD on the African convection in summer 1984. This is associated with a modulation of the low-level zonal wind component off the West African coast (solid line in Fig. 9d) whose enhanced westerly component is in phase or lags by 1 or 2 day the convective enhancement due to the QBZD. The wavelet diagram (Fig. 9a) also shows enhanced activity of Kelvin waves especially in June and the first half of July.

Figure 9e presents a longitude–time diagram of the 3-hourly CLAUS brightness temperature (blue shading) field and of the daily Kelvin band filtered OLR (green contours) both averaged over 2.5° – 12.5° N from 1 June to 31 July 1984. The CLAUS data enable us to follow westward trajectories of MCS from East Africa to the west as far as the Gulf of Mexico. It can also be seen that the level of activity over Africa is variable, along with the westward extension of the MCS trajectories. This activity can also vary along the track of individual MCSs. The Kelvin wave activity has been delineated when the related filtered OLR signal is higher than 10 W m^{-2} in absolute value. Several wave trains are detected crossing from West to East Africa in particular. We note an interesting modulation of MCS activity by the passage of a Kelvin wave train, with the negative (positive) OLR phase of the wave enhancing (weakening) convection in the MCS. In Mounier et al. (2007) it was shown that Kelvin waves significantly modulate the convective intensity of individual westward propagating MCSs through an eastward displacement of their “convective envelope.” In particular, Mounier et al. (2007) analyzed in detail the Kelvin event from 1 and 10 July 1984 (see Fig. 9 of their paper). It shows the enhancement of the MCS activity (from the high-resolution dataset) over the eastern Atlantic and Africa when the Kelvin wave crosses this domain as well as a strong modulation of rainfall in the African ITCZ.

Also shown in Fig. 9e is the activity of the QBZD dipole (red rectangles). These rectangles are based on QBZD index peaks greater than one standard deviation in absolute value (Fig. 9d) and depict the space–time areas of the QBZD dipole [solid (dashed) contours for positive (negative) OLR anomalies]. As for the modulation of the MCS by the Kelvin waves, we see that the QBZD negative (positive) phases are associated with the enhancement (weakening) of the convec-

tive intensity of the embedded MCS. In particular, the highest modulation by the QBZD occurs on 10 July (Fig. 9e). The impact of the QBZD on the MCS activity at this time is dramatic. An envelope of highly enhanced convection is located over West Africa and is associated with the absence of any significant convective activity over the central and western Atlantic during the following days partly due to the development of the western opposite pole of the QBZD dipole. Finally, when considering the Kelvin wave tracks along with the space–time location of the QBZD poles, we see that during most of the time positive (negative) phases of the Kelvin waves link western and eastern positive (negative) QBZD poles.

Let us now focus on the African monsoon onset (3 July) and its interactions with the QBZD and the occurrence of Kelvin waves. The sequence from 30 June to 13 July corresponds with the combined occurrence of a Kelvin wave train and the high activity of the QBZD. Just before this onset on 3 July, we observe a temporary decrease of convection over the whole of West Africa (Figs. 9b,c), which is a primary characteristic of onset for this monsoon system (Sultan and Janicot 2003). This suppressed-convective sequence corresponds both to the occurrence of a positive OLR contribution from the QBZD and the arrival over West Africa of a positive OLR phase of a Kelvin wave (Fig. 9e). The crossing of this Kelvin wave train during the sequence 1–10 July has been detailed in Mounier et al. (2007) and is associated with an enhancement of the low-level easterly wind component off the coast of West Africa, decreasing the moisture advection inland (Fig. 9d). This is followed by the negative phase of the Kelvin wave crossing the whole longitude domain, partly linking the western negative OLR pole of the QBZD with the eastern negative OLR pole of the following opposite phase of the QBZD. Consequently, convective activity in the African ITCZ is enhanced after 5 July in phase with the

←

FIG. 9. The case study of the 1984 African monsoon season. (a) Wavelet diagram for indices computed over the ITCZ area (2.5° – 12.5° N, 10° W– 10° E) from 1 May to 30 Sep 1984: shaded, ITCZ index based on raw OLR (red contours); QBZD index (green contours); ITCZ index based on OLR filtered for the Kelvin wave signal; the figure covers the period of 2.5–36 days. (b) Latitude–time diagram of daily rainfall (mm day^{-1}) from 1 Jun to 31 Jul 1984 over the latitude domain 5° – 12.5° N, averaged over 10° W– 10° E and filtered to remove variability lower than 10 days (values greater than 5 mm day^{-1} are shaded). (c) Same as (b), but for OLR (values lower than 230 W m^{-2} are shaded) in the latitude domain 0° – 15° N. The location of the Guinean coast is displayed as a horizontal line at 5° N. (d) QBZD standardized time series (open circles) and mean 925-hPa standardized zonal wind averaged over 0° – 20° N, 25° W– 0° (solid line) from 1 Jun to 31 Jul 1984. (e) Longitude–time diagram from 1 Jun to 31 Jul 1984 of 3-hourly CLAUS brightness temperature (K, blue shading) and of daily Kelvin band filtered OLR (green contours, W m^{-2}), both averaged over the latitude 2.5° – 12.5° N. The longitude area 10° W– 10° E is delineated. The two green dashed lines in (b) and (c) depict the occurrence of the negative OLR phase of the Kelvin wave over West Africa at the time of the monsoon onset transition period. The red rectangles in (e) are based on the QBZD index peaks and depict the space–time areas of the QBZD dipole [solid (dashed) contours for positive (negative) OLR anomalies]. The two red dashed lines in (b) and (c) depict the occurrence of the negative OLR phase of the QBZD over West Africa [corresponding to red circles in (d)] at the time of the monsoon onset transition period.

enhancement of the low-level westerly wind component off the West African coast (Fig. 9d). The sequences of occurrence of the negative phases of both Kelvin wave (green lines) and QBZD (red lines) over West Africa are represented in Figs. 9b and 9c. Both the QBZD and the Kelvin wave are preceded by easterly wind anomalies and followed by westerly wind anomalies. It appears that the Kelvin wave accounts for the first part of the transition period of the monsoon onset, contributing to increase convection both over the Guinean Coast and the Sahelian latitudes, while the QBZD phase is responsible for the second part of this transition period by maintaining a high level of convection over the Sahelian latitudes. We thus suggest that a Kelvin wave train combined with the QBZD triggered the monsoon onset process over Africa in 1984. A last point of interest is that the negative Kelvin phase is immediately followed by the positive one, still superimposed on the negative pole of the QBZD (dotted red rectangle centered on 10 July). Figure 9e shows clearly the temporary decrease of convective activity over Africa due to the positive Kelvin phase, but it is not strong enough to weaken the global convective activity in this rectangle, and convection reactivates immediately after the passage of the positive phase. This demonstrates that due to a shorter space–time scale, a Kelvin wave can modulate convection within the QBZD pole over Africa without modifying the primary character of the convective intensity controlled by the QBZD.

The monsoon onset of 1984 has been presented as a case study possibly favorable to interactions with the QBZD and Kelvin wave occurrences since the ITCZ is located more equatorward relative to the mean during the summer, when convective activity can excite equatorial waves more strongly. Mounier (2005) showed that the Kelvin wave activity as well as the projection of OLR values on the QBZD is higher during northern spring when the ITCZ is centered on the equator. Similarly, Nguyen (2007) showed that the Kelvin wave is the main synoptic-scale system over central Africa in March–April. So it appears that it is during the first rainy season between April and June, at the time of the monsoon onset before the ITCZ “jumps” to the north that equatorial dynamics interacts best with convective activity in the African ITCZ. The summer monsoon onsets over West Africa have not been systematically studied in detail over the last 25 yr but individual wavelet diagrams of OLR have been computed (Mounier 2005). Peaks in the QBZD spectral energy can be noticed at the time of the monsoon onset for other years like 1981, 1987, 1988, 1989, 1990, 1994, 1997, 1998, 1999, and 2000 (not

shown). Similarly, activity in the Kelvin spectral signal can also be detected during some monsoon onsets but a more detailed investigation, beyond the scope of this study, would be needed to be able to compare those evolutions with that during 1984.

6. Conclusions

We have investigated the mechanisms giving rise to the main intraseasonal mode of convection in the African monsoon during northern summer, which we refer to as the quasi-biweekly zonal dipole (QBZD). Its mean periodicity is centered around 12–14 days but it varies between 10 and 25 days. The QBZD is primarily characterized by a quasi-stationary zonal dipole of convection whose dimension is larger than the West African monsoon domain with the two poles centered respectively along the Guinean coast and between 30° and 60°W in the equatorial Atlantic. The QBZD is associated with a Walker-type vertical circulation in a near-equatorial zonal plane. It is controlled both by equatorial atmospheric dynamics through a Kelvin wave–type disturbance propagating eastward between its two poles and by land surface processes over Africa, inducing combined fluctuations in surface temperatures, surface pressures, and low-level zonal winds off the coast of West Africa. When convection is at a minimum over central and West Africa, reduced cloud cover induces higher net shortwave flux at the surface, which increases surface temperatures and lowers surface pressures. This induces an east–west pressure gradient both around the latitudes of the ITCZ (10°N) and of the Saharan heat low (20°N), leading to an increase in eastward moisture advection inland. The arrival from the Atlantic of the positive pressure signal associated with a Kelvin wave pattern amplifies the low-level westerly wind component and the moisture advection inland, leading to an increase in convective activity over central and West Africa at the peak of the oscillation. Then the opposite phase of the dipole develops. The role of surface fluxes may be crucial in setting the time scale of the QBZD, as was hypothesized for a similar mode observed during northern spring by Grodsky and Carton (2001). Examination of surface temperature, moisture, and flux data from the African Monsoon Multidisciplinary Analysis (AMMA) field program during summer 2006, when some QBZD occurrences have been observed, may provide a useful basis to test this hypothesis.

The propagation of the convective envelope and of the associated 200-hPa velocity potential anomalies is also detected from the eastern Pacific to the Indian

Ocean, covering a longitude band from approximately 120°W to 90°E. Figure 3 depicts the teleconnection pattern in the 200-hPa velocity potential field. Similar modes of northern summer variability including Africa have been detected previously both at interannual and decadal time scales (Janicot et al. 2001; Chen et al. 2001; Chelliah and Bell 2004). In particular, the decadal time-scale pattern (Fig. 3c of Chelliah and Bell 2004) highlights negative–positive–negative 200-hPa velocity potential poles over equatorial America–Africa–south-east Asia, similar to those of the QBZD. This might indicate some systematic organization of Walker-type circulations in the vertical–zonal plane at different time scales, linking a portion of the monsoon system activity over these three continents.

When the effect of the Kelvin wave propagation is removed by filtering, the stationary character of the QBZD is highlighted. This demonstrates that the QBZD is composed 1) of a stationary dipole whose interactions with surface processes are strong and 2) by Kelvin wave dynamics linking the western pole of the QBZD to its eastern pole of the same sign with a time lag of about 5 days. One possible scenario is that Kelvin wave activity can excite large-scale convection over Africa if the surface flux field is primed, in turn exciting the lower-frequency QBZD mode. This type of scenario appears to occur occasionally during monsoon onset, when the large-scale pressure, temperature, and moisture gradients are set up for monsoon convection and a Kelvin wave acts as a trigger for onset. This appears to have happened during the West African monsoon onset in 1984.

Acknowledgments. We are thankful to the NOAA–CIRES Climate Diagnostics Center (Boulder, Colorado) for providing the NCEP–NCAR reanalysis dataset and the interpolated OLR dataset from their Web site (<http://www.cdc.noaa.gov/>). We thank also Henri Laurent (LTHE, IRD) for providing the daily rainfall dataset and the cloud cluster dataset. We warmly thank the three reviewers who provided us with a very detailed examination of our draft. Based on French initiative, AMMA was built by an international scientific group and is currently funded by a large number of agencies, especially those from France, United Kingdom, United States, and Africa. It has been the beneficiary of a major financial contribution from the European Community's Sixth Framework Research Programme. Detailed information on scientific coordination and funding is available on the AMMA International Web site (<http://www.amma-international.org>). GNK was supported by NOAA's Climate Program Office under Grant GC05-156.

REFERENCES

- Arkin, P. A., 1979: The relationship between fractional coverage of high cloud and rainfall accumulations during GATE over the B-scale array. *Mon. Wea. Rev.*, **107**, 1382–1387.
- Cattell, R. B., 1966: The scree test for the number of factors. *Multivariate Behav. Res.*, **1**, 245–276.
- Chelliah, M., and G. D. Bell, 2004: Tropical multidecadal and interannual climate variability in the NCEP–NCAR reanalysis. *J. Climate*, **17**, 1777–1803.
- Chen, T.-C., J. Yoon, K. J. St. Croix, and E. S. Takle, 2001: Suppressing impacts of the Amazonian deforestation by the global circulation change. *Bull. Amer. Meteor. Soc.*, **82**, 2209–2216.
- Diedhiou, A., S. Janicot, A. Viltard, P. de Felice, and H. Laurent, 1999: Easterly wave regimes and associated convection over West Africa and tropical Atlantic: Results from the NCEP/NCAR and ECMWF reanalyses. *Climate Dyn.*, **15**, 795–822.
- Duvel, J. P., 1989: Convection over tropical Africa and the Atlantic ocean during northern summer. Part I: Interannual and diurnal variations. *Mon. Wea. Rev.*, **117**, 2782–2799.
- , 1990: Convection over tropical Africa and the Atlantic ocean during northern summer. Part II: Modulation by easterly waves. *Mon. Wea. Rev.*, **118**, 1855–1868.
- Folland, C. K., T. N. Palmer, and D. E. Parker, 1986: Sahel rainfall and worldwide sea temperatures 1901–85. *Nature*, **320**, 602–607.
- Giannini, A., R. Saravanan, and P. Chang, 2003: Oceanic forcing of Sahel rainfall on interannual to interdecadal time scales. *Science*, **302**, 1027–1030.
- Grodsky, S. A., and J. A. Carton, 2001: Coupled land/atmosphere interactions in the West African monsoon. *Geophys. Res. Lett.*, **28**, 1503–1506.
- Grueber, A., and A. F. Krueger, 1984: The status of the NOAA outgoing longwave radiation data set. *Bull. Amer. Meteor. Soc.*, **65**, 958–962.
- Hall, N. M. J., G. N. Kiladis, and C. D. Thorncroft, 2006: Three-dimensional structure and dynamics of African easterly waves. Part II: Dynamical modes. *J. Atmos. Sci.*, **63**, 2231–2245.
- Hastenrath, S., 1991: *Climate Dynamics of the Tropics*. Kluwer, 488 pp.
- Hodges, K. I., and C. D. Thorncroft, 1997: Distribution and statistics of African mesoscale convective weather systems based on the ISCCP Meteosat imagery. *Mon. Wea. Rev.*, **125**, 2821–2837.
- , D. W. Chappell, G. J. Robinson, and G. Yang, 2000: An improved algorithm for generating global window brightness temperatures from multiple satellite infrared imagery. *J. Atmos. Oceanic Technol.*, **17**, 1296–1312.
- Janicot, S., and B. Sultan, 2001: Intraseasonal modulation of convection in the West African monsoon. *Geophys. Res. Lett.*, **28**, 523–526.
- , S. Trzaska, and I. Poccard, 2001: Summer Sahel-ENSO teleconnection and decadal time scale SST variations. *Climate Dyn.*, **18**, 303–320.
- Kalnay, E., and Coauthors, 1996: The NCEP/NCAR 40-Year Reanalysis Project. *Bull. Amer. Meteor. Soc.*, **77**, 437–471.
- Kanamitsu, M., W. Ebisuzaki, J. Woollen, S.-K. Yang, J. J. Hnilo, M. Fiorino, and G. L. Potter, 2002: NCEP–DOE AMIP-II reanalysis (R-2). *Bull. Amer. Meteor. Soc.*, **83**, 1631–1643.
- Kiladis, G. N., and K. M. Weickmann, 1997: Horizontal structure and seasonality of large-scale circulations associated with

- submonthly tropical convection. *Mon. Wea. Rev.*, **125**, 1997–2013.
- , C. D. Thorncroft, and N. M. J. Hall, 2006: Three-dimensional structure and dynamics of African easterly waves. Part I: Observations. *J. Atmos. Sci.*, **63**, 2212–2230.
- Knutson, T. R., and K. M. Weickmann, 1987: 30–60 day atmospheric oscillations: Composite life cycles of convection and circulation anomalies. *Mon. Wea. Rev.*, **115**, 1407–1436.
- Laing, A. G., and J. M. Fritsch, 1993: Mesoscale convective complexes in Africa. *Mon. Wea. Rev.*, **121**, 2254–2263.
- , and —, 1997: The global population of mesoscale convective complexes. *Quart. J. Roy. Meteor. Soc.*, **123**, 389–405.
- Lamb, P. J., 1978a: Case studies of tropical Atlantic surface circulation patterns during recent sub-Saharan weather anomalies: 1967 and 1968. *Mon. Wea. Rev.*, **106**, 482–491.
- , 1978b: Large-scale tropical surface circulation patterns associated with sub-Saharan weather anomalies. *Tellus*, **30**, 240–251.
- , R. A. Peppler, and S. Hastenrath, 1986: Interannual variability in the tropical Atlantic. *Nature*, **322**, 238–240.
- Le Barbé, L., T. Lebel, and D. Tapsoba, 2002: Rainfall variability in West Africa during the years 1950–90. *J. Climate*, **15**, 187–202.
- Liebmann, B., and C. A. Smith, 1996: Description of a complete (interpolated) outgoing longwave radiation dataset. *Bull. Amer. Meteor. Soc.*, **77**, 1275–1277.
- Mathon, V., and H. Laurent, 2001: Life cycle of Sahelian mesoscale convective cloud systems. *Quart. J. Roy. Meteor. Soc.*, **127**, 377–406.
- , —, and T. Lebel, 2002: Mesoscale convective system rainfall in the Sahel. *J. Appl. Meteor.*, **41**, 1081–1092.
- Mathews, A. J., 2004: Intraseasonal variability over tropical Africa during northern summer. *J. Climate*, **17**, 2427–2440.
- Mekonnen, A., C. D. Thorncroft, and A. R. Aiyer, 2006: Analysis of convection and its association with African easterly waves. *J. Climate*, **19**, 5405–5421.
- Mounier, F., 2005: La variabilité intersaisonnière de la mousson d’Afrique de l’Ouest et Centrale. Ph.D. thesis, Université Pierre et Marie Curie, 259 pp.
- , and S. Janicot, 2004: Evidence of two independent modes of convection at intraseasonal timescale in the West African summer monsoon. *Geophys. Res. Lett.*, **31**, L16116, doi:10.1029/2004GL020665.
- , G. N. Kiladis, and S. Janicot, 2007: Analysis of the dominant mode of convectively coupled Kelvin waves in the West African monsoon. *J. Climate*, **20**, 1487–1503.
- Newell, R. E., and J. Kidson, 1984: African mean wind changes between Sahelian wet and dry periods. *Int. J. Climatol.*, **4**, 27–33.
- Nguyen, T. T. H., 2007: Analyses des perturbations synoptiques et de la modulation diurne des systèmes convectifs sur l’Afrique centrale. Ph.D. thesis, Université Pierre et Marie Curie, 254 pp.
- Nicholson, S. E., 1978: Climatic variations in the Sahel and other African regions during the past five centuries. *J. Arid Environ.*, **1**, 3–24.
- North, G. R., T. L. Bell, R. F. Cahalan, and F. J. Moeng, 1982: Sampling errors in the estimation of empirical orthogonal functions. *Mon. Wea. Rev.*, **110**, 699–706.
- Reed, R. J., D. C. Norquist, and E. E. Recker, 1977: The structure and properties of African wave disturbances as observed during Phase III of GATE. *Mon. Wea. Rev.*, **105**, 317–333.
- Richman, M. B., 1986: Rotation of principal components. *Int. J. Climatol.*, **6**, 293–335.
- Rossow, W. B., A. Walker, and M. Roiter, 1997: International Satellite Cloud Climatology Project (ISCCP) description of reduced resolution radiance data. WMO Tech. Doc. 58, World Meteorological Organization, 163 pp.
- Roundy, P. E., and W. M. Frank, 2004: A climatology of waves in the equatorial region. *J. Atmos. Sci.*, **61**, 2105–2132.
- Rowell, D. P., 2001: Teleconnections between the tropical Pacific and the Sahel. *Quart. J. Roy. Meteor. Soc.*, **127**, 1683–1706.
- , C. K. Folland, K. Maskell, and M. N. Ward, 1995: Variability of summer rainfall over tropical North Africa (1906–92): Observations and modelling. *Quart. J. Roy. Meteor. Soc.*, **121**, 669–704.
- Straub, K. H., and G. N. Kiladis, 2002: Observations of a convectively coupled Kelvin wave in the eastern Pacific ITCZ. *J. Atmos. Sci.*, **59**, 30–53.
- Sultan, B., and S. Janicot, 2000: Abrupt shift of the ITCZ over West Africa and intraseasonal variability. *Geophys. Res. Lett.*, **27**, 3353–3356.
- , and —, 2003: The West African monsoon dynamics. Part II: The “preonset” and “onset” of the summer monsoon. *J. Climate*, **16**, 3407–3427.
- , —, and A. Diedhiou, 2003: The West African monsoon dynamics. Part I: Documentation of intraseasonal variability. *J. Climate*, **16**, 3389–3406.
- Thompson, R. M., Jr., S. W. Payne, E. E. Recker, and R. J. Reed, 1979: Structure and properties of synoptic-scale wave disturbances in the intertropical convergence zone of the eastern Atlantic. *J. Atmos. Sci.*, **36**, 53–72.
- Thorncroft, C. D., and B. J. Hoskins, 1994a: An idealized study of African easterly waves. Part I: A linear view. *Quart. J. Roy. Meteor. Soc.*, **120**, 953–982.
- , and —, 1994b: An idealized study of African easterly waves. Part II: A nonlinear view. *Quart. J. Roy. Meteor. Soc.*, **120**, 983–1015.
- Torrence, C., and G. P. Compo, 1998: A practical guide to wavelet analysis. *Bull. Amer. Meteor. Soc.*, **79**, 61–78.
- Wang, H., and R. Fu, 2007: The influence of Amazon rainfall on the Atlantic ITCZ through convectively coupled Kelvin waves. *J. Climate*, **20**, 1188–1201.
- Ward, M. N., 1998: Diagnosis and short lead time prediction of summer rainfall in tropical North Africa at interannual and multidecadal timescales. *J. Climate*, **11**, 3167–3191.
- Wheeler, M., G. N. Kiladis, and P. J. Webster, 2000: Large scale dynamical fields associated with convectively coupled equatorial waves. *J. Atmos. Sci.*, **57**, 613–640.
- Yang, G.-Y., and J. Slingo, 2001: The diurnal cycle in the tropics. *Mon. Wea. Rev.*, **129**, 784–801.